
Article:
Bates, L and Bradley, D (2017) Deflagrative, Auto-ignitive, and Detonative Propagation Regimes in Engines. Combustion and Flame, 175. pp. 118-122. ISSN: 0010-2180

https://doi.org/10.1016/j.combustflame.2016.05.023

Deflagrative, Auto-ignitive, and Detonative Propagation Regimes in Engines

L. Bates and D. Bradley*

School of Mechanical Engineering, University of Leeds, LS2 9JT, UK

**Corresponding author. E-mail address: d.bradley @leeds.ac.uk*

Abstract

The paper presents a novel overall quantitative description of the major regimes of engine combustion, covering the influences of both turbulence and auto-ignition parameters on burn rates and flame extinctions. It involves two separate, yet interconnected, correlation diagrams. The first involves the normalised turbulent burning velocity, the Karlovitz stretch factor the strain rate Markstein number, and also includes possible the relative auto-ignitve burn rates. The second is a complementary correlating ξ / ε diagram, involving the auto-ignitve parameters of ignition delay and excitation times. The ξ parameter is the acoustic speed normalised by the auto-ignition velocity, while ε is the acoustic wave residence time in a hot spot, normalised by the excitation, or heat release, time. It also includes an indication of the regime of normal flame propagation. The different auto-ignitive regimes, in which a variety of contrasting fuel/air mixtures might operate, are indicated on the ξ / ε diagram, particularly in relation to its peninsula of developing detonation at a hot spot. Operational points, measured on a variety of engines, are also shown on the two diagrams, in terms of the different regimes, including those of mild and "super-knock", turbulent flame extinctions, and controlled auto-ignition.

Keywords: Octane numbers, Ignition delay times, Excitation times, Hot Spots, Developing detonation, Burning velocities, Engine knock.

Nomencature

a	acoustic speed (m s^{-1})	U	turbulent burning velocity normalised by rms turbulent velocity.
c	dimensionless constant with given values of u_l, a, l and v.	u_a	autoignition velocity (m s^{-1})
E	activation energy (J mol^{-1})	u_l	laminar burning velocity (m s^{-1})
$\bar{E}$	detonation stability dimensionless group, ($\bar{E}=(\tau_i/\tau_e)(E/RT)$)	u_t	turbulent burning velocity (m s^{-1})
K	Karlovitz turbulent flame stretch factor	u'	rms turbulent velocity (ms^{-1})
l	turbulent length scale (m)	***Greek***	
Ma_{sr}	strain rate Markstein number	ε	Residence time of pressure wave in hot spot normalised by excitation time ($\varepsilon = r_o/a\tau_e$).
P	Pressure (Pa)	v	Kinematic viscosity (m^2 s^{-1})
R	ideal gas constant (J mol^{-1} K^{-1})	ξ	Acoustic speed normalised by autoignition velocity ($\xi = a/u_a$).
R	distance along r_o (m)	τ_e	Excitation time (s)

r_o	hot spot radius (m)	τ_i	Ignition delay time (s)
$\bar{r}$	normalised hotspot radius	ϕ	Equivalence ratio
T	temperature (K)		

1. Introduction

It was first proposed in 1927 AD to base the rating of gasoline engine fuels on the performance of mixtures of the Primary Reference Fuels, PRF, *i*-octane and *n*-heptane. With the aim of rating the fuel, rather than the engine, in the early 1930s a standardised variable compression engine was developed for the measurement of the Research and Motor Octane Numbers, RON and MON. However, *i*-octane and *n*-heptane, are now inadequate surrogates for the extensive variety of potential contemporary fuels, and it is difficult to isolate fuel rating from engine performance. In addition, the operational engine pressures, temperatures, and equivalence ratios are very different from those in the Cooperative Fuels Research, CFR, engines used for measuring RON and MON, with their different inlet charge temperatures [1].

These changes in fuels and engines have led to the development of alternative surrogate fuels to the PRFs [2] and the use of measured Octane Indices, OI, related to ONs through empirical *K* factors, in such expressions as [3]:

$$\text{OI} = \text{RON} - K(\text{RON} - \text{MON}). \quad (1)$$

Another approach has been to employ ignition delay and excitation times, embodied in the developing detonation peninsula regime, plotted on a diagram of ξ / ε coordinates [4]. Here ξ is the acoustic speed, a, normalised by the auto-ignition velocity, u_a, and ε is the acoustic wave residence time in the auto-igniting hot spot, normalised by the excitation time, τ_e. This time is the duration of the energy release, after the auto-ignition delay time, τ_i, has elapsed. If sufficient energy feeds into the acoustic wave a detonation develops. Engine operational loci can be plotted on such a diagram and entry of these into this detonation peninsula is indicative of possible severe engine knock developing at hot spots. Other regimes of auto-ignitive combustion can also be indicated on the ξ / ε diagram, including those of benign controlled auto-ignition. Recently, Robert et al. [5]

have demonstrated how the diagram shows increasing the spark advance, increases the number of operational loci moving to within the peninsula, with increasingly severe engine knock.

A complete understanding of the various combustion regimes requires an additional complementary diagram that can indicate the different regimes of both turbulent and auto-ignitive combustion, including those of flame extinction. Regimes of turbulent combustion, are shown on the *U/K* diagram [6], where *K* is not to be confused with the *K* in Eq. (1). Here, *U* is the turbulent burning velocity, u_t, normalised by the rms turbulent velocity, u' , and *K* is the Karlovitz turbulent flame stretch factor. The present study develops the overlapping links between these two diagrams and synthesises a new diagram that is indicative of both turbulent and auto-ignitive, pre-mixed, combustion regimes. It includes the relative magnitudes of turbulent burning velocity and auto-ignitive velocity that can arise at a possible igniting hot spot.

In addition, the ξ / ε diagram, with an indication of the boundary between hot spot autoignitive/deflagrative boundary, is used first to assess the propensity of different fuels to auto-ignite and, if so, to characterise the auto-ignition, and identify engine operational regimes, including "super-knock."

2. ξ and the *U/K* diagram

The auto-ignitve velocity, u_a, is driven by a reactivity gradient, arising from localised spatial gradients of temperature, specie concentrations, or both. Only the temperature gradient is considered here, and it is in terms of such gradients creating those of τ_i. These are at localised spherical hot spots, radius, r_o. This creates an auto-ignition velo city, u_a, expressed by

$$u_a = \partial r / \partial \tau_i = (\partial r / \partial T)(\partial T / \partial \tau_i) . \quad (2)$$

With an activation temperature, *E/R,* at temperature *T,* and constant pressure, the Arrhenius equation yields:

$$\partial \tau_i / \partial T = \tau_i \left(E / RT^2 \right), \text{ and} \quad (3)$$

$$\xi = a/u_a = a(\partial T / \partial r)(\partial \tau_i / \partial T) . \quad (4)$$

Evaluation of ξ requires values of τ_i for the appropriate mixtures over the operational ranges of pressure, *P,* and temperature. Detonations and severe engine knock are associated with the auto-ignitive front propagating at close to the acoustic speed, and with ξ consequently close to unity. Shown on Fig. 1 are some values of ξ, calculated from Eq. (4), using the τ_i data sources referenced in the caption, for stoichiometric mixtures of different fuels with air at 4 MPa, and a temperature gradient of -2K/mm. Of interest, are the strikingly superior anti-knock properties of CH_4, H_2 and H_2/CO below 950K, and of toluene and ethanol. Ethanol has lower values of ξ below 960K than toluene despite having a lower RON value because of a relatively high $\partial\tau_i/\partial T$ which gives ethanol a lower value of u_a. OI 105 refers to the Octane Index of a surrogate gasoline fuel, with a volumetric composition of 62% *i*-octane, 29% toluene and 9% n-heptane and a RON of 98 [7]. This surrogate fuel gives significantly higher values of ξ at temperatures below about 900K than PRF 98.

On the *U/K* diagram in [5], *U* is expressed in terms of both the Karlovitz stretch factor, *K*, which embodies the laminar burning velocity, u_l, the integral length scale of the turbulence, *l*, the kinematic viscosity ν, and also of the strain rate Markstein number, $Ma_{sr,}$ where

$$K = 0.25\left(u'/u_l\right)^2\left(u'l/\nu\right)^{-0.5} \text{ and} \tag{5}$$

This gives rise to the expression that relates turbulent to laminar burning velocities:

$$u_t/u_l = U\left[4K\left(u_l l/\nu\right)^{0.5}\right]^{2/3} \tag{6}$$

With $\xi = a/u_a$, and division by u_a:

$$\left(u_t/u_a\right) = U\left(4K\right)^{2/3}\left(ul/\nu\right)^{1/3}\left(u_l\xi/a\right), \text{ and} \tag{7}$$

$$\left(u_t/u_a\xi\right) = U\left(4K\right)^{2/3}c, \text{ where } c = \left(u_l/a\right)\left(u_l l/\nu\right)^{1/3}, \text{ characterising in-cylinder properties.} \tag{8}$$

The ratio of deflagrative to auto-ignitive propagation velocity, u_t/u_a, is an indicator of which of these is dominant in the propagation of reaction initiated at a hot spot. It has been employed in both direct numerical simulations, DNS, and experiments [13,14]. Values of *c* were found from estimated values of u_l, *a*, *l* and *v* within the peninsula, with u_l = 0.4 ms^{-1}, *a* = 510 ms^{-1}, *l* = 0.002 m, and *v* = 1.5.10 $^{-5}$ m^2s^{-1}. These give *c* = of 0.00636.

Contours of both $(u_t/u_a\xi)$ and Ma_{sr} are plotted on the new synthesised diagram of plots of U against K, in Fig. 2, based on this value of c. For a different value of c, say c', the revised value for the contour would be that on Fig. 2 multiplied by $c'/0.00636$. Over most of the diagram, mixed combustion is possible, dependent on the value of ξ. Within the flame quench regime only auto-ignitive burning is possible.

A condition curve of turbulent burning during isentropic compression is shown dotted and arrowed, on Fig. 2. This is based on the turbulent burning velocity of a stoichiometric *i*-octane/air up to the knocking condition at 10 MPa, with u' = 3 m/s and l = 2 mm. Laminar burning velocity and Ma_{sr} data are extrapolated from those in [15]. Such data at high P, and T are rather more sparse than are τ_i data. The condition curve cuts the ($u_t/u_a\xi$) contour at a value of 0.005. Consequently, even with ξ = 10, the u_t/u_a ratio would only be 0.05 and auto-ignitive propagation would prevail at any sufficiently active hot spot. Here the dominant influence is that of ξ. In contrast, under atmospheric conditions ξ would be very large and u_t would dominate. A more complete understanding of the deflagrative/auto-ignitive regimes and their burning rates must be supplemented by the ξ/ε diagram.

3. The ξ/ε diagram for different fuels

The value of ε is a measure of the energy transfer into the developing acoustic front at a hot spot, expressed by:

$\varepsilon = r_o/a\tau_e$, where r_o is the hot spot radius. (9)

The higher the value of ε, the greater is the reinforcement of the potentially damaging acoustic wave.

The construction of the ξ/ε diagram, shown in Fig. 3, resulted from many direct numerical simulations of hot spot auto-ignition, based on detailed chemical kinetics in [4], and in one of Norbert Peter's last papers, [16]. Within the peninsula, bounded by lower and upper limits, ξ_l and ξ_u, hot spot auto-ignition might lead to a developing detonation. The figure also shows regimes of thermal explosion and sub-sonic auto-ignition. After the low values of ε at the toe of the peninsula, an increase in its value increases ξ_u, increasing the depth of the peninsula, as a result of the stronger pressure pulses. In [16], it is shown that:

$\xi\varepsilon = -\bar{E}(\partial \ln T \partial/\bar{r})$, in which $\bar{E} = (\tau_i/\tau_e)E/RT$ and $\bar{r} = r/r_o$. (10)

When $\bar{E}(\partial \ln T \partial/\bar{r})$ exceeds 1500, at the higher values of ξ, deflagration becomes significantly more probable than auto-ignition [16]. This relationship and that for a lower value of $\bar{E}(\partial \ln T \partial/\bar{r})$ = 50, extensively within the peninsula, are shown in Fig. 3. The lower values of $\bar{E}(\partial \ln T \partial/\bar{r})$ are associated with smaller temperature gradients.

The dotted and arrowed condition curve for turbulent burning is similarly shown in Fig. 3 between these two limit curves. This demonstrates that the initial propagation from a hot spot could be sub-sonic prior to entering into the peninsula.

The prime purpose of Fig. 3 is to assess the propensity of different fuel/air mixtures to develop a detonation after hot spot auto-ignition, during isentropic compression from 800K and 0.1 to 10 MPa and, ultimately, 1100K at 15 MPa. Dashed curves cover the later stage of compression between 10 and 15 MPa, associated with combustion regimes in turbo-charged engines. Data sources of τ_i and τ_e for the different *P* and *T,* are given in Table 1. Sometimes the limited data on τ_e necessitated extrapolations of existing data. This was especially so in the case of CH_4, with its restricted pressure range, for which the data were among the first τ_e data to be calculated. [11]. The low temperature and pressure conditions of the available data made it necessary to compute new detailed chemical kinetic values for CH_4 excitation times [17]. Mixtures studied include H_2/air, at an equivalence ratio, ϕ , = 0.45, equi-moles of H_2 and CO and with air, mixtures of growing importance for reducing solid state iron ore to iron, at, ϕ = 0.5 and 0.6, together with a PRF of 95, at ϕ = 1.0.

DNS reveal that hot spots exist in a variety of sizes and shapes, and that the assumed spherical shape is an idealisation [13,18]. In the present context, those sizes and shape that auto-ignite within the detonation peninsula are most relevant. In [7] engine geometric considerations suggested r_o = 5 mm, and *dr/dT* = -2 K/mm. The value of E_n for heavy knock was estimated to be 7,000 in [16]. With *dr/dT* = -2 K/mm, this gives a value of $\bar{E}(\partial \ln T \partial/\bar{r})$ = 17.5, which is consistent with its location within the toe of the peninsula in Fig. 3. Together with the consistency of the available engine and fuel test results for a variety of engines and fuels, this confirmed the suitability of these hot spot values, for bench marking engine knock in Figs. 3 and 4.

All fuels were mixed with air. None of the H_2 or H_2/CO mixture conditions, even at the higher pressures, enter the detonation peninsula. Similarly, CH_4 largely avoids the peninsula, only crossing into the region of developing detonation under severe conditions and with high values of ε. It was not possible to calculate the characteristics for alcohol fuels, due to a lack of data on their values of τ_e.

The 95 PRF, ϕ = 1, entered the detonation peninsula at a pressure of 6 MPa and 925K, whereas the surrogate gasoline, OI = 105, ϕ = 1, RON = 98, was able to attain a pressure exceeding 7.5 MPa and a temperature of 950K prior to such entry. Not only does the latter mixture have a superior anti-knock performance, but it is an interesting example of a negative value of *K* in Eq. (1), with an OI value that is higher than the RON rating of the fuel.

4. The ξ / ε diagram for different engines

Figure 4 shows data on engine knock and near-knock, drawn from a variety of studies. Table 2 gives the symbols for type of engine, sources of data, the fuels, auto-ignitive modes, maximum pressures and temperatures. Some data are new [19, 20], some have been employed in earlier studies [1, 21-25]. Engine types included controlled auto-ignition, conventional spark ignition, turbo charged, and a rapid compression machine, RCM. Operational points at the highest cylinder pressures are shown in the figure. A **+** indicates controlled auto-ignition, an unfilled symbol no knock, a half-filled symbol moderate knock, and a filled symbol "super-knock" induced by pre-ignition. In general, an increase in pressure increased the severity of knock. All operations with controlled auto-ignition were at ϕ = 0.25, with PRF 84 fuel, and exhaust gas recirculation, to attain a sufficient temperature for auto-ignition. Otherwise ϕ = 1.0.

Data points indicated by Δ are from a rapid compression machine, in which maximum knock pressure amplitudes varied as $\xi^{-1.923}$, close to the estimate of ξ^{-2} in [26]. The diverse operational conditions show that entry into the detonation peninsula is associated with the onset of knock, which can become severe

Conclusions

1. The combined *U/K* and ξ / ε diagrams indicate the different regimes of combustion. In particular, entry into the detonation peninsula is a good indicator of knock severity.

2. The ξ / ε diagram, based on τ_i and τ_e data is a better predictor of auto-ignition and engine knock than RON and MON values. This is illustrated by regimes of negative *K* values in Eq. (1), in which the knock resistance measured by an OI value is higher than the RON value.

3. The combined diagrams are particularly effective in identifying operational regimes for controlled auto-ignition engines.

4. It is demonstrated how H_2, H_2/CO, CH_4 and ethanol are effective anti-knocks, as is toluene, in the lower temperature range.

5. Advantageous negative values of *K* in Eq. (1) arise partly from the greater charge cooling that arises in modern engines, and partly from the smaller inverse exponent for, non-PRF, realistic fuels [1,3], that determines the effect of pressure on τ_i.

Acknowledgements

Thanks are expressed to Inna Gorbatenko for the computation of CH_4 excitation times from detailed chemical kinetics and to EPSRC for the award of a Research Studentship to L.B. The help of Norbert Peters also is acknowledged, through enjoyable discussions on several of the aspects covered in the present paper.

References

1. D. Bradley, R.A Head, Engine autoignition: The relationship between octane numbers and autoignition delay times. Combust. Flame 147 (2006) 171-184.

2. N. Morgan, A. Smallbone. A. Bhave, M. Kraft, R. Cracknell, G. Kalghatgi, Mapping surrogate gasoline compositions into RON/MON space. Combust. Flame 157 (2010) 1122-1131.

3. G.T. Kalghatgi, Developments in internal combustion engines and implications for combustion science and future transport fuels. Proc. Combust. Inst. 35 (2015) 101-115.

4. X.J. Gu, D.R. Emerson, D. Bradley, Modes of reaction front propagation from hot spots. Combust. Flame 133 (2003) 63–74.

5. A. Robert, S. Richard, O. Colin, T. Poinsot, LES study of deflagration to detonation mechanisms in a downsized spark ignition engine. Combust. Flame 162 (2015) 2788-2807.

6. D. Bradley M. Lawes, Kexin Liu, M.S. Mansour, MS Measurements and correlations of turbulent burning velocities over wide ranges of fuels and elevated pressures. Proc. Combust. Inst. 34 (2013) 1519–1526.

7. G.T. Kalghatgi, D. Bradley, J. Andrae, A.J. Harrison, Internal Combustion Engines: Performance, Fuel Economy and Emissions. (2009) IMechE London, UK, 8-9 December 2009, Institution of Mechanical Engineers.

8. N. Peters, B. Kerschens, G. Paczko, Super-Knock Prediction Using a Refined Theory of Turbulence. SAE paper 2013-01-1109, (2019).
9. Gaurav Mittal, Sinéad M. Burke, Varun A. Davies, Bikash Parajuli, Wayne K. Metcalfe, Henry J. Curran, Autoignition of ethanol in a rapid compression machine, Combust. Flame 161 (2014) 1164-1171.10. D.F. Davidson, M.M. Gauthier, R.K. Hanson, Shock tube ignition measurements of iso-octane/air and toluene/air at high pressures. Proc. Combust. Inst. 30 (2005) 1175-1182.
11. A.E. Lutz, R.J. Kee, J.A. Miller, H.A. Dwyer, A.K. Oppenheim, Dynamic effects of autoignition centers for hydrogen and C1, 2-hydrocarbon fuels. Twenty-Second Symposium (International) on Combustion/The Combustion Institute (1988) pp. 1683-1693.
12. S. Browne, Z. Liang, J.E. Shepherd, Detailed and simplified chemical reaction mechanisms for detonation simulation. Fall 2005 Western States Section of the Combustion Institute (2005).
13. R. Sankaran, Hong. G. Im, E.R. Hawkes, J.H. Chen, The effects of non-uniform temperature distribution on the ignition of a lean homogeneous hydrogen–air mixture. Proc. Combust. Inst. 30 (2005) 875-882.
14. A.B. Mansfield, M.S. Wooldridge, High-pressure low-temperature ignition behavior of syngas mixtures. Combust. Flame 161 (2014) 2242-2251.
15. D. Bradley, R.A. Hicks, M. Lawes, C.G.W. Sheppard, R. Woolley, The Measurement of Laminar Burning Velocities and Markstein Numbers for Iso-octane–Air and Iso-octane–n-Heptane–Air Mixtures at Elevated Temperatures and Pressures in an Explosion Bomb. Combust. Flame 115 (1998) 126-144.
16. L. Bates, D. Bradley, G. Paczko, N. Peters, “Engine Hot Spots: Modes of Auto-ignition and Reaction Propagation," Combust. Flame 166 (2016) 80-85.
17. I. Gorbatenko, University of Leeds, Private communication.
18. Chun Sang Yoo, Tianfeng Lu, Jacqueline H. Chen, Chung K. Law, Direct numerical simulations of ignition of a lean n-heptane/air mixture with temperature inhomogeneities at constant volume: Parametric study. Combust. Flame 158 (2011) 1727-1741.
19. J. Rudloff, J.M. Zaccardi, S. Richard, J.M. Anderlohr, Proc. Combust. Inst.34 (2013) 2959-2967. Proc. Combust. Inst.34 (2013) 2959-2967.
20. Kimitoshi Tanoue, Yuichi Chado, Taishu Jimoto, Takashi Nomura, Fumio Shimada, Jun Hashimoto, Effect of autoignition characteristics of fuels on knocking properties. International J of Engine Research September 1, (2015) 1468087415601785.
21. D. Bradley, Autoignitions and detonations in engines and ducts. Phil. Trans. Royal Soc. A 370 (2012) 689-714.
22. P. Rothenberger, GM Powertrain, Germany, Private Communication [21].
23. Z. Wang, H. Liu, T. Song, Y. Xu, J.X. Wang, Investigation on Pre-ignition and Super-Knock in Highly Boosted Gasoline Direct Injection Engines. SAE paper 2014-01-1212 (2014). 14
24. Z.Wang, H. Liu, T. Song, Y. Qi, X.He, S. Shuai, J.X. Wang, Relationship between super-knock and pre-ignition. Int. J. Engine Research. 16 (2015) 166-180.
25. P.W. Manz, VW Germany, Private Communication [21]

26. D. Bradley, G.T. Kalghatgi, Influence of autoignition delay time characteristics of different fuels on pressure waves and knock in reciprocating engines. Combust. Flame 156 (2009) 2307-2318.

List of Figure Captions

Fig. 1. Calculated values of ξ at 4 MPa and $\partial T/\partial r$ = -2 K/mm for stoichiometric mixtures of air with: OI 105 [6], PRFs [1,8], ethanol [9], toluene [10], methane [11], hydrogen [12].

Fig. 2. Turbulent and auto-ignitive burning regimes on a *U/K* diagram, with contours of Ma_{sr} and $\left(u_t/u_a\xi\right)$.

Fig. 3. Isentropic compression curves for different fuels showing propensity for detonation. Solid curves indicate compression from 800K to 1000K at ≈10 MPa. Broken curves show continuation of this compression to 1100K at 15 MPa, relevant to turbo charged engines.

Fig. 4. Engine operational points close to maxima *P* and *T* for different engines and fuels, as listed in Table 2, which gives the key to symbols, + indicates controlled auto-ignition. Increasing black fill of symbols indicates increasing knock intensity, with fully filled symbols indicating "super-knock", semi-filled symbols a relatively small knock and un-filled symbols no knock.

List of Table Captions

Table 1. Table 1. Sources of data for τ_i and τ_e between 3 and 15 MPa, 800 and 1100K.

Table 2. Engine data relevant to Fig. 4. Symbols indicate operational points in figure..

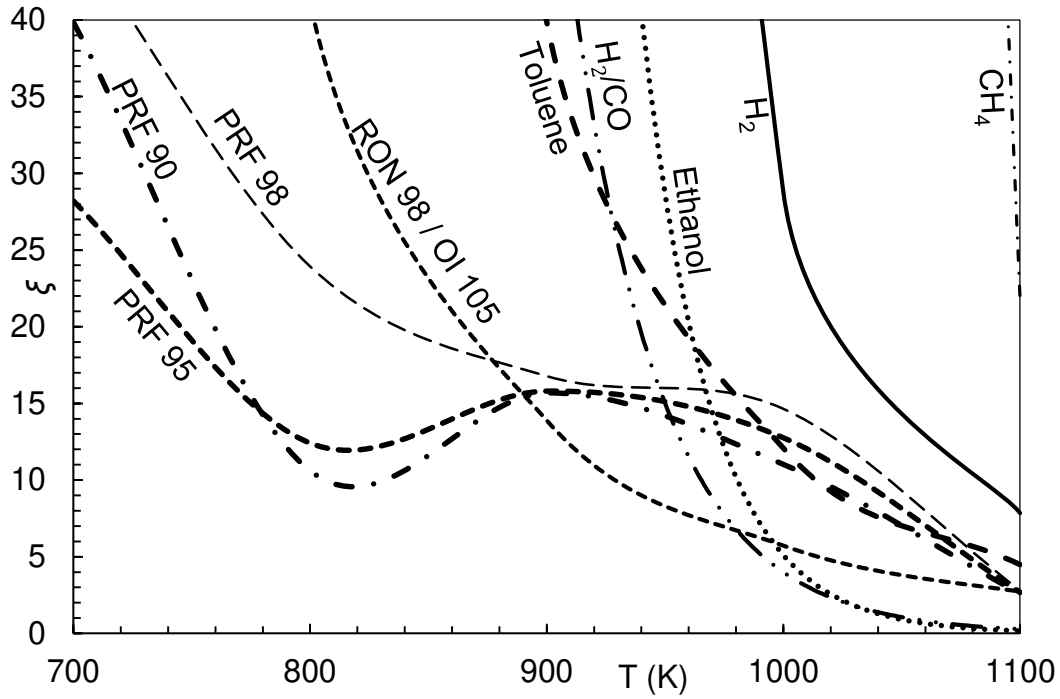

Figure 1. Calculated values of ξ at 4 MPa and $\partial T/\partial r$ = -2 K/mm for stoichiometric mixtures of air with: OI 105 [6], PRFs [1,8], ethanol [9], toluene [10], methane [11], hydrogen [12].

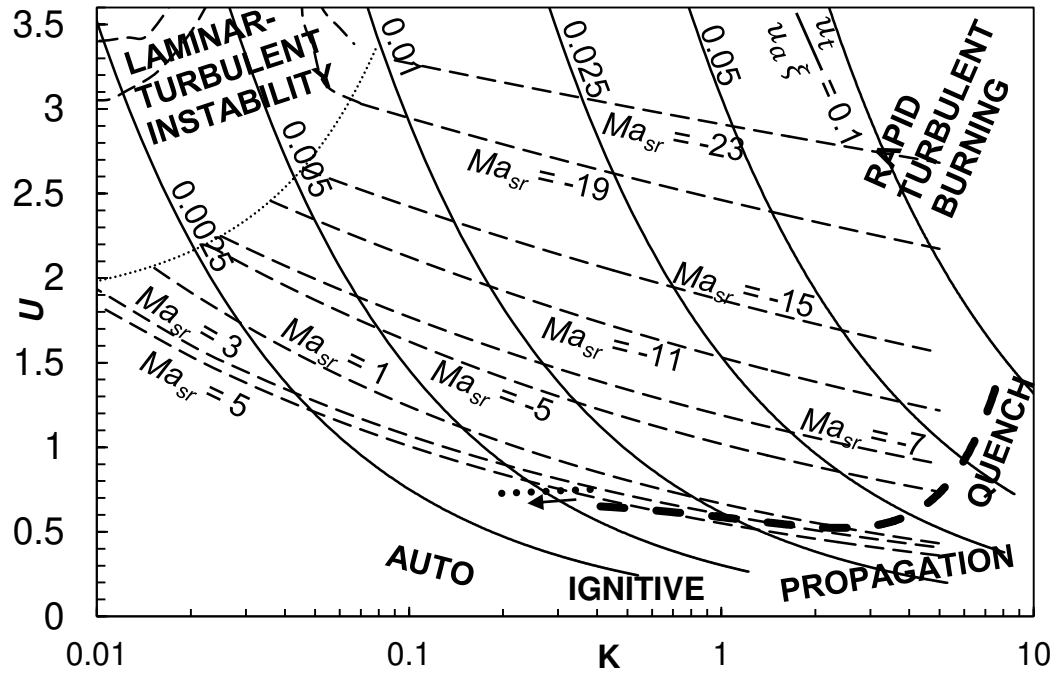

Figure. 2. Turbulent and auto-ignitive burning regimes on a *U/K* diagram, with contours of Ma_{sr} and $\left(u_t/u_a\xi\right)$.

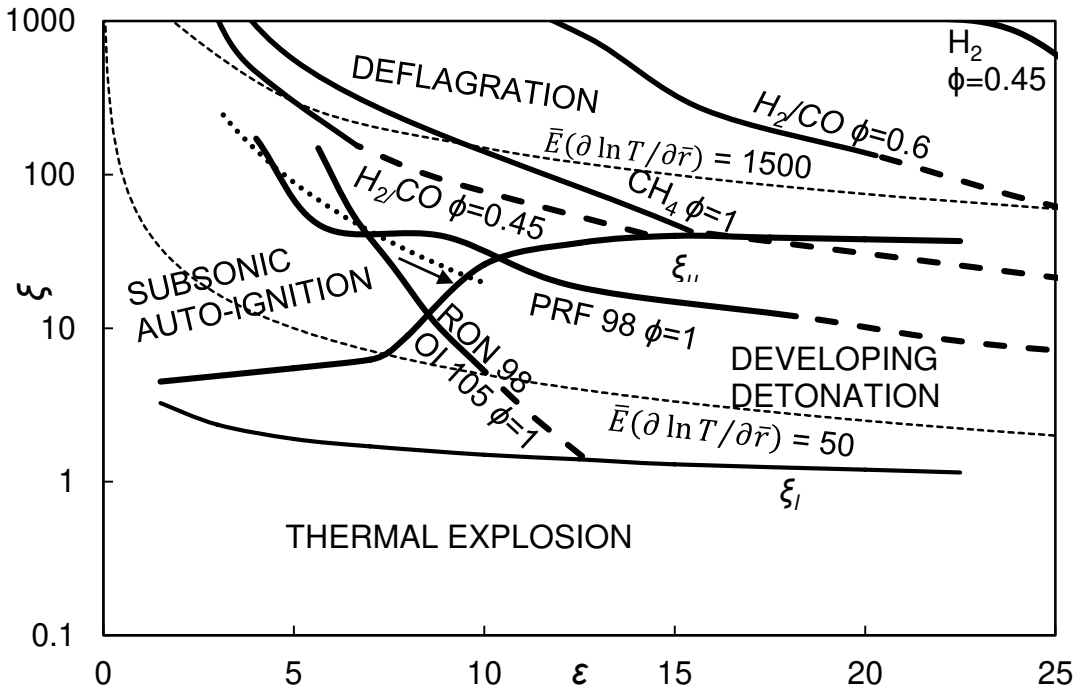

Figure 3. Isentropic compression curves for different fuels showing propensity for detonation. Solid curves indicate compression from 800K to 1000K at ≈10 MPa. Broken curves show continuation of this compression to 1100K at 15 MPa, relevant to turbo charged engines.

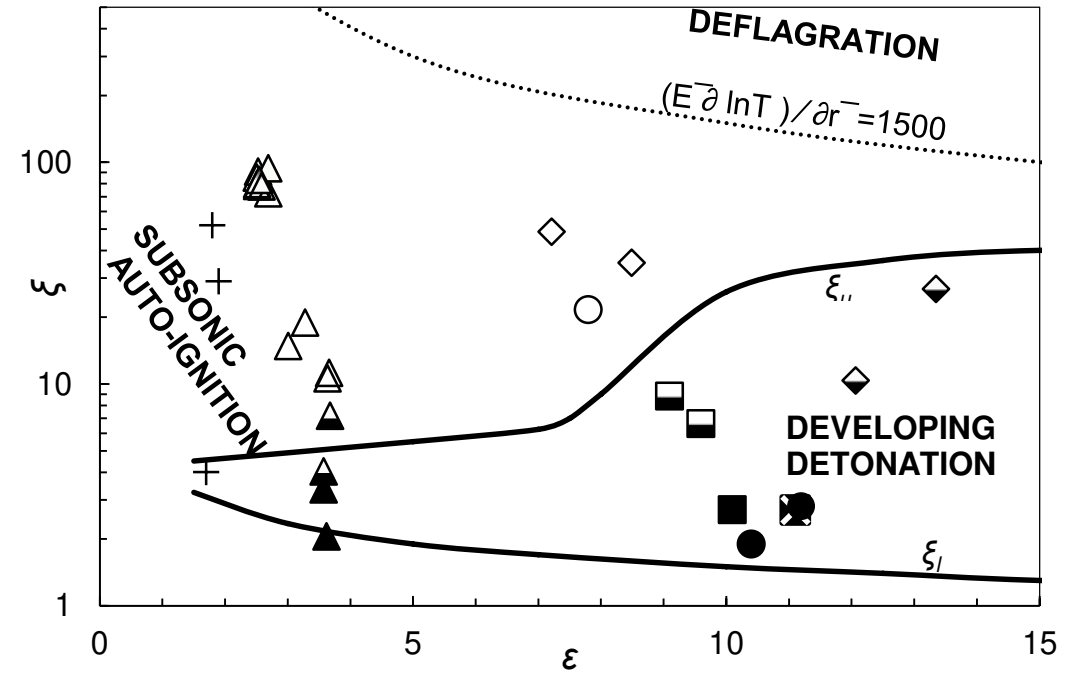

Figure 4. Engine operational points close to maxima *P* and *T* for different engines and fuels, as listed in Table 2, which gives the key to symbols, + indicates controlled auto-ignition. Increasing black fill of symbols indicates increasing knock intensity, with fully filled symbols indicating "super-knock", semi-filled symbols a relatively small knock and un-filled symbols no knock.

Fuel	ϕ	τ_i	τ_e
H_2/CO	0.5, 0.6	[4]	[4]
H_2	0.45	[12]	[12]
PRF 100, 98, 95	1	[1,8]	[8]
CH_4	1	[11,17]	[11,17]
OI 105	1	[7]	[7]

Table 1. Sources of data for τ_i and τ_e between 3 and 15 MPa, 800 and 1100K.

Symbol	Type	Fuel	Autoignitive Mode	*P* MPa (max)	*T* K (max)	Ref.
+	Single cylinder – Roots blower	PRF 84 ϕ = 0.25	Controlled auto-ignition	6.52	729	[1,21]
◊	Single cylinder	RON 97	Deflagration - superknock	2.74	1000 (estim.)	[19]
Δ	RCM	C_4H_{10} with DME addititive	Deflagration - superknock	5.55	835	[20]
○	S.I. engine -turbo	RON 95 / OI. 105	Deflagration - superknock	12.8	1057	[22]
□	S.I. engine -turbo	RON 94	Light knock - superknock	10.91	949	[23,24]
×	S.I. engine -turbo	RON 98 / OI. 107	Superknock	13.3	926	[25]

Table 2. Engine data relevant to Fig. 4. Symbols indicate operational points in figure.